NANOSYSTEMS: PHYSICS, CHEMISTRY, MATHEMATICS, 2013, 4 (2), P. 196–205

X-RAY DIFFRACTION STUDY OF THE PHASE AND MORPHOLOGY CHANGES IN YTTRIUM COMPOUND NANOPARTICLES

R. P. Ermakov, V. V. Voronov, P. P. Fedorov

A. M. Prokhorov General Physics Institute, Russian Academy of Sciences, Moscow, Russia

x-ray_diffraction@mail.ru

In the present experimental study, the precipitation of basic yttrium nitrate from aqueous solutions allowed the optimization of conditions for the preparation of loosely aggregated $Y_2(OH)_5NO_3 \cdot 1.5H_2O$, the thermal decomposition of which, under controlled annealing, permitted the synthesis of yttria nanoparticles with desirable microstructure. The latter material can be widely used to manufacture yttria optical ceramics. $Y_2(OH)_5NO_3 \cdot 1.5H_2O$ thermolysis occurs via the formation of a metastable hexagonal Y_2O_3-based phase ($a = 8.04$, $c = 12.37$ Å).

Keywords: yttrium oxide, optical ceramics, X-ray diffraction phase analysis.

1. Introduction

The preparation of laser nanoceramics with spectral and lasing properties similar to that of single crystals is one of the most important innovations in the field of optical materials in recent years [1]. Advantages of ceramic materials over single crystals include improved mechanical properties, increased laser sustainability, ability to synthesize large samples, monotonous and homogeneous distribution of the high-concentration dopants, opportunity to obtain transparent optical media when the preparation of the single crystals is obstructed, ability to produce multilayered elements, etc. Neodymium- and/or ytterbium-doped yttrium oxide ceramics have spectral and lasing properties very close to the properties of alumoyttrium garnet (YAG) [2]. However, preparation of the former compounds in single crystal form is hindered by the polymorphic phase transition which occurs at temperatures close to its melting point and the high melting temperature of the aforementioned materials. Thus, a shift from single crystal growth to a polycrystalline technology is one of the most promising avenues for the manufacture of yttria-based active laser elements. In fact, the ThO_2-stabilized ceramic Y_2O_3:Nd^{3+} was the first polycrystalline oxide laser material developed [3].

The study of synthetic methods and precursors for the preparation of yttria-based laser ceramics continues at a very accelerated pace [4–12] because these materials possess high chemical stability, high transparency in the IR region, low thermal expansion and high heat conductivity [13]. Activated yttria powders can also be used as luminophores [14].

Transparent oxide ceramics synthesis includes the preparation of precursors with designated composition and morphology. Each step of this procedure is crucially important for the quality of the final product. One should closely monitor and control the size of domains with coherent scattering, narrow size distribution of such domains, low agglomeration, low defect concentration and high chemical purity. These parameters are linked to the sample microstructure, and thus, can be studied by full-profile X-ray diffraction phase analysis.

Therefore, the subject of this paper was the optimization of these conditions for the preparation of the yttria precursor by its precipitation from aqueous nitrate solutions, determination of the correlations between preparation conditions and product microstructure and control over the latter.

2. Experimental

Yttria samples with controlled properties were prepared in two steps. The first step included the synthesis of basic yttrium nitrate. Commercially available 99.99% pure Y_2O_3 was dissolved in a slight excess of diluted nitric acid (15 wt.%; 99.9% pure) under heating. Then the formed solution was carefully titrated with aqueous ammonia (pH = 9.60; prepared by dilution of concentrated 99.9% pure NH_4OH with double-distilled water) under stirring. Precipitation of white jelly-like basic yttrium nitrate during the titration was controlled by the HANNA INSTRUMENT pH-meter (pH = 0.76–9.00). The second step included the thermal decomposition of the obtained precipitate and formation of yttria. Sample thermolysis was performed in SNOL ovens (alumina crucibles; 100 mg specimens). All experiments were performed under air unless specified otherwise.

Thermal decomposition conditions were determined by thermogravimetry (Q-1500D derivatograph; quartz crucibles; 50–100 mg samples ($\pm$ 0.4 mg); Pt–Pt/Rh thermocouples; heating rate of 10 °C/min in the 25–600 °C range ($\pm$ 2 °C)).

X-Ray diffraction experiments were done with the use of DRON-4 diffractometer (CuKα radiation; Maud software, RITA/RISTA method [15–19]). We used silicon powder as an internal standard for the evaluation of the instrumentation functions.

Leo 912 AB Omega electron microscope was used for the investigation of the specimen microstructure.

3. Results and Discussion

3.1. Preparation and Analysis of Precursor

As previously mentioned in the Experimental section, preparation of the yttria precursor was carried out in two steps. The first step included dissolution of Y_2O_3 and formation of acidic aqueous nitrate solution:

$$Y_2O_3 + 6HNO_3 = 2Y(NO_3)_3 + 3H_2O. \quad (1)$$

Then yttrium hydroxynitrate, the precursor of yttria powder with controlled properties, was precipitated by direct titration with aqueous ammonia:

$$2Y(NO_3)_3 + (6 - x)NH_4OH + nH_2O = Y_2(OH)_{6-x}(NO_3)_x \cdot nH_2O + (6 - x)NH_4NO_3. \quad (2)$$

A typical titration curve for the reaction of aqueous $Y(NO_3)_3$ and NH_4OH is presented in Fig. 1. It has two low-slope steps "a–b" and "c–d". Both correspond to the precipitation of yttrium hydroxynitrate $Y_2(OH)_{6-x}(NO_3)_x{\cdot}nH_2O$. $Y_2(OH)_{6-x}(NO_3)_x{\cdot}nH_2O$ precipitates might have had different compositions (i.e., x values) at different steps of the titration curve (Fig. 1). Therefore, we studied properties of $Y_2(OH)_{6-x}(NO_3)_x{\cdot}nH_2O$, formed at each step, separately, i.e., at each step (between points "a" and "b" at pH 6.8, and at the end of titration at point "d", pH 9.4), precipitates were isolated from the matrix solution and studied separately after filtering, washing and drying.

Concerning the specimens' flowability, samples prepared at different pH values had different degrees of agglomeration; precipitates obtained at pH 6.8 had rigid agglomerates, whereas specimens precipitated at pH 9.0 had loose agglomerates. We continue to investigate the cause of this difference.

Both types of these samples have identical X-ray diffraction patterns, similar to the pattern of $Y_2(OH)_5NO_3{\cdot}1.5H_2O$ phase (JCPDS card 49-1107) and $Y_2(OH)_{5.14}(NO_3)_{0.86}\cdot H_2O$ phase

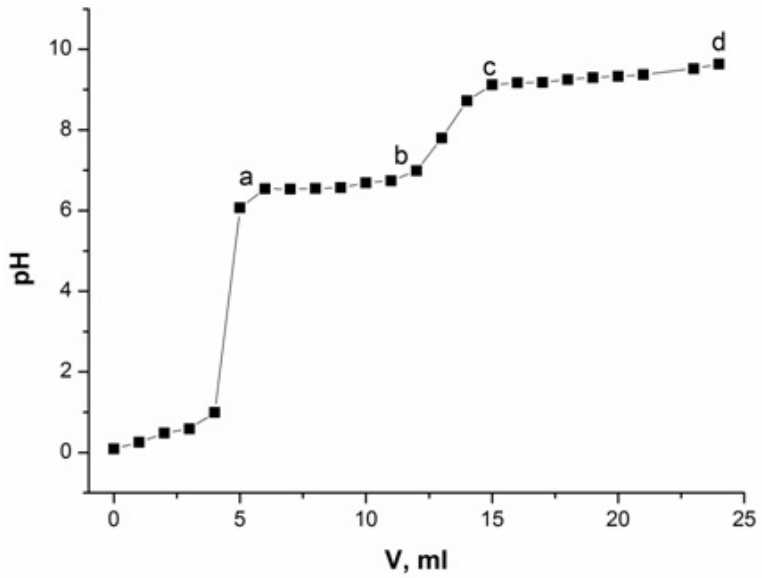

FIG. 1. pH value of the titrated 0.20 M $Y(NO_3)_3$ solution vs. amount of NH_4OH added (ml)

TABLE 1. X-Ray diffraction pattern of $Y_2(OH)_{6-x}(NO_3)_x \cdot nH_2O$ basic nitrate

2Θ, degrees	**d, Å**	$\mathbf{Q_{exp}}$	$\mathbf{I/I_0}$**, a.u.**	**(hkl)**	$\mathbf{Q_{calc}}$	**ΔQ**
9.63	9.182	118.60	100	(002)	119.95	–1.35
19.53	4.546	483.83	33	(004)	479.81	4.02
20.49	4.335	532.02	13	(113)	529.69	2.33
28.10	3.175	991.79	30	(040)	996.55	–4.75
28.75	3.105	1037.18	60	(220)	1039.18	–2.00
30.24	2.956	1144.71	15	(016)	1141.86	2.85
33.20	2.699	1373.00	9	(231)	1380.59	–7.59
34.62	2.591	1489.18	10	(051)	1587.09	–3.46
35.73	2.513	1583.63	11	(320)	2026.73	3.37
40.65	2.219	2030.10	11	(236)	2430.17	–7.01
44.61	2.031	2423.17	11	(260)	3032.27	–8.46
50.17	1.819	3023.81	19	(139)	3187.12	–13.88
51.48	1.775	3173.24	18	(420)	3409.30	–4.12
53.47	1.714	3405.18	8	(080)	3986.19	–9.24
58.18	1.586	3976.95	8	(440)	4156.71	–3.36

[JCPDS card 32-1435]. These data were indexed in orthorhombic crystal lattice ($a = 17.115(5)$ Å, $b = 12.67(1)$ Å, $c = 18.26(1)$ Å) (Fig. 2, Table 1).

Analysis of the obtained X-ray diffraction patterns confirmed that the precipitates are of a single phase only, but reflections in these patterns have different profiles. Reflections formed by (200) planes are much wider than those formed by (211) planes, perhaps, because of

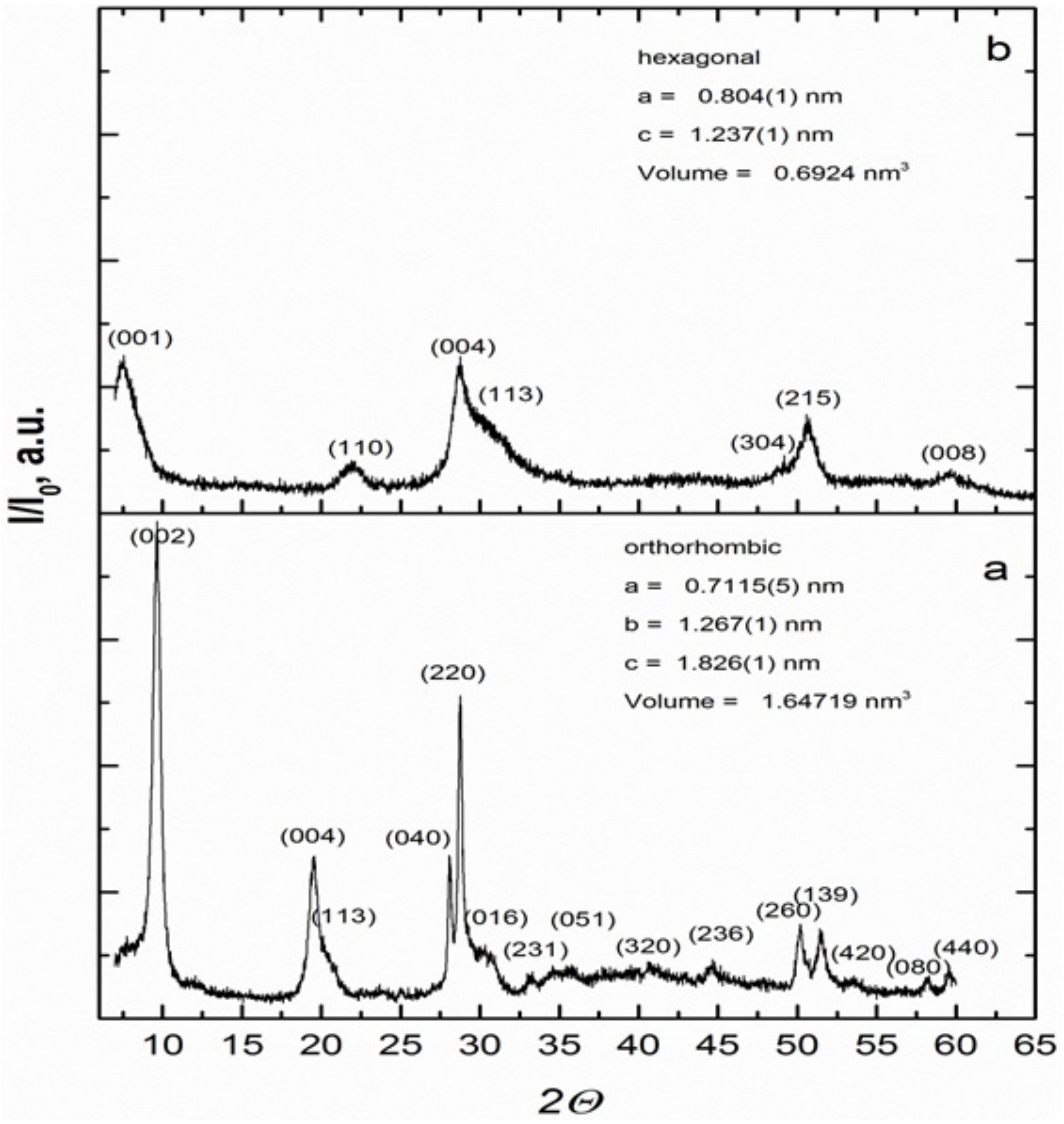

FIG. 2. X-Ray diffraction patterns of $Y_2(OH)_{6-x}(NO_3)_x \cdot nH_2O$ basic nitrate (a) and novel hexagonal Y_2O_3-based phase (b)

anisotropy of the coherent scattering domains. This was confirmed by electron microscopy data (Fig. 3), the particles have planar shape.

3.2. Thermal Decomposition of Basic Yttrium Nitrate with the Formation of Yttria

In order to prepare yttria starting materials which are ready to be used for further ceramics synthesis, the precursor ($Y_2(OH)_{6-x}(NO_3)_x \cdot nH_2O$) is to be thermolyzed to Y_2O_3. Thermolysis of this precursor (precipitated at pH 9.0) yielded the thermogravimetric data shown in Fig. 4.

Thermolysis of $Y_2(OH)_{6-x}(NO_3)_x \cdot nH_2O$ is a multistep process (Fig. 4) that includes five distinguishable endothermic steps which sometimes overlap.

There was no mass loss observed above 600 °C. This is in agreement with data [9].

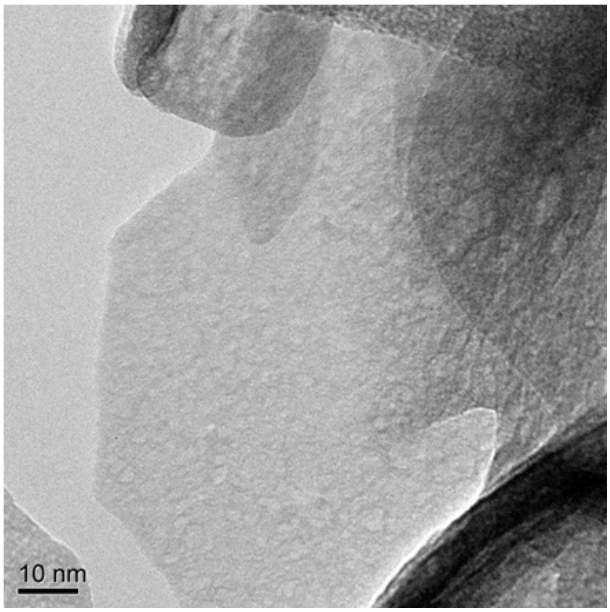

FIG. 3. Electron microscopy image of $Y_2(OH)_{6-x}(NO_3)_x \cdot nH_2O$ basic nitrate precipitate

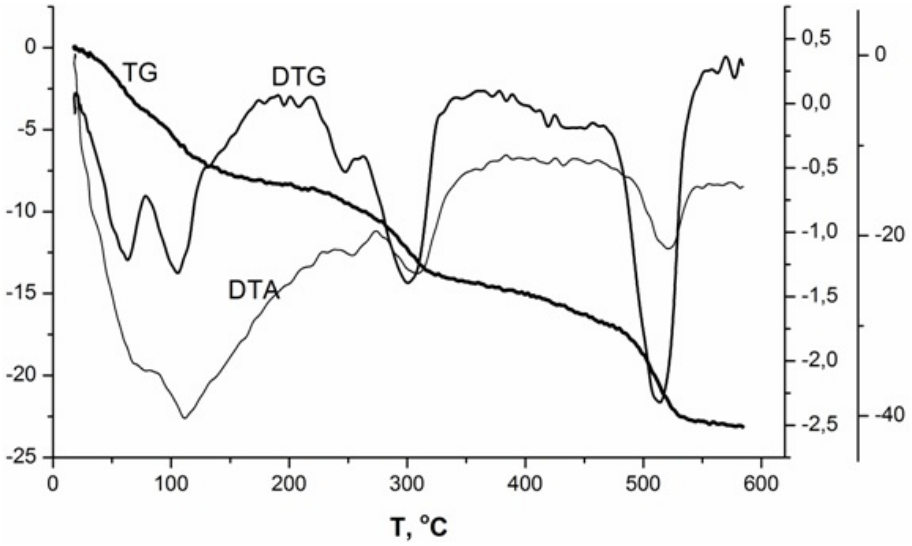

FIG. 4. Thermogravigram of basic yttrium nitrate thermal decomposition

4. Changes in Morphological Properties of Yttria Nanoparticles

4.1. Transformation under Slow Heating

As has already been mentioned, strict control over the microstructure properties of the prepared powders is a must in order to assure the final products will have the proper quality. One widely used means of such control is the thermal treatment of the samples. We used a full-profile X-ray diffraction phase analysis to study the correlation between the sample microstructure and manner of its thermal treatment.

X-Ray diffraction patterns of the samples heated at 2.5 °C/min rate in 20–900 °C interval are presented in Fig. 5 for the samples heated to 500, 600, 700, 800 and 900 °C (please

remember that the thermal decomposition of $Y_2(OH)_{6-x}(NO_3)_x \cdot nH_2O$ and its conversion to Y_2O_3 should be complete above 500–600 °C (Fig. 4)).

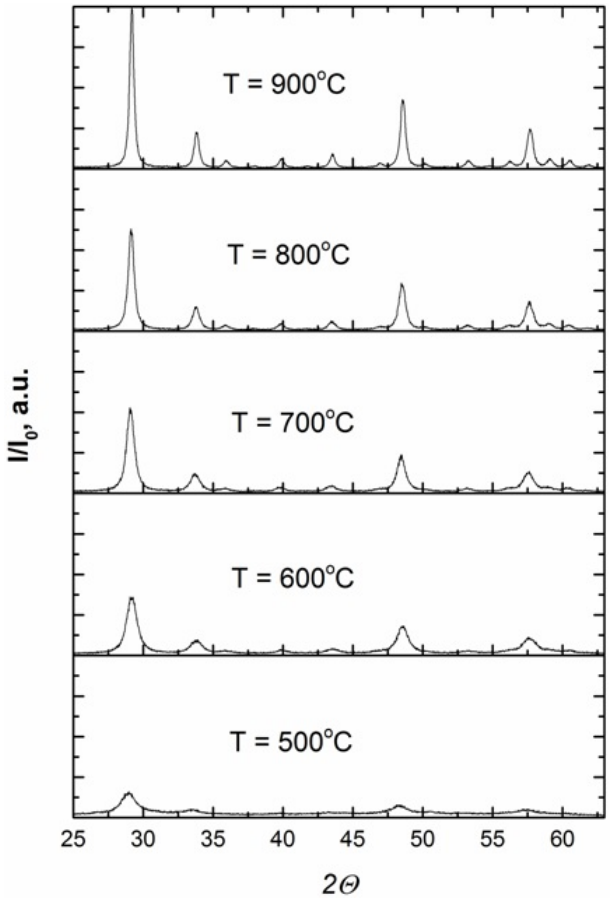

FIG. 5. X-Ray diffraction patterns of yttria samples heated to 500, 600, 700, 800 and 900 °

One can easily notice the changes in the reflection profiles for the X-ray diffraction patterns. The higher the heating temperature, the lower the half-width of the peaks, and the higher the reflection intensity. Correlations between the sizes of the coherent scattering domains and microdeformations as functions of the temperature are presented in Fig. 6. The average size of coherent scattering domains grew linearly, while microdeformations decreased with increasing temperature.

4.2. Isothermal Annealing

A more thorough study of the influence that the heating temperature has on the microstructure changes of yttria nanopowders was performed using isothermal annealing.

With 600 °C annealing (0.5–1.400 min.), the formation of a novel phase similar to $Y_2(OH)_{6-x}(NO_3)_x \cdot nH_2O$ basic nitrate was observed. This phase had a simpler X-ray diffraction pattern (Fig. 2b) and can be indexed in the hexagonal system ($a = 8.04(1)$ Å, $c = 12.37(1)$ Å; Table 2). A similar X-ray pattern was observed for the sample of basic yttria nitrate precursor, heated to 500 °C at a rate of 10 °C/min (see Fig. 3d in [9]).

However, for annealing times exceeding 3 minutes, the X-ray diffraction patterns of the thermolysis products contained exclusively reflections of cubic Y_2O_3 phase (Fig. 7). Increasing the annealing times of the latter resulted in an increase in the maximum intensity of the lines

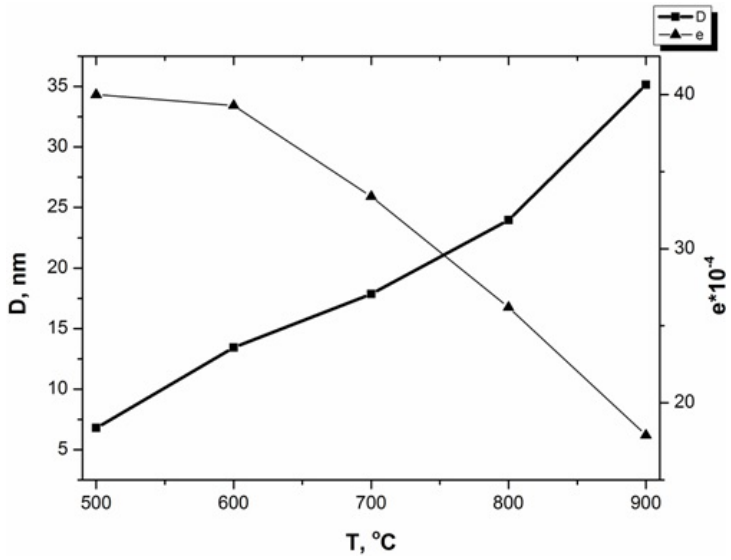

FIG. 6. Correlation between the size of domains of coherent scattering (squares) or microdeformations (triangles) and attained temperature (2.5 °C/min heating rate)

TABLE 2. X-Ray diffraction pattern of the novel Y_2O_3–based phase

2Θ, degrees	**d_{exp}, Å**	**Q_{exp}**	**I/I_0, a.u.**	**(hkl)**	**Q_{calc}**	**ΔQ**
7.49	11.793	71.90	100	(001)	65.46	6.44
21.96	4.044	611.39	30	(110)	618.80	–7.41
28.73	3.105	1037.36	95	(004)	1047.33	–9.97
31.11	2.873	1211.94	50	(113)	1207.92	4.02
49.00	1.858	2898.25	25	(304)	2903.72	–5.47
50.66	1.800	3084.79	55	(215)	3080.31	4.48
59.78	1.546	4185.30	20	(008)	4189.32	–4.02

and a decrease of their half-width (Fig. 7). This means that the sample microstructure changed, with an increase of the crystalline phase content; extension of the annealing time increased the size of the coherent scattering domains (Fig. 8). The average size of these domains changed in a non-linear manner with increased annealing times, doubling in size in the first 5 hours, and then slowing down. (Fig. 8).

Changes in the X-ray diffraction patterns of yttria samples and the corresponding changes in the microstructure parameters are presented in Figs. 9 and 10, respectively. It is worth noting that the sizes of the coherent scattering domains for the samples annealed at 800 °C are more than twice the size of samples heated at 600 °C for the same time. Similarly, samples annealed at 800 °C have three times fewer microdeformations than specimens annealed at 600 °C. These facts unequivocally demonstrate that the microstructure of yttria nanopowders can be controlled by both annealing time and temperature.

5. Conclusions

The present experimental study which examined the precipitation of basic yttrium nitrate from aqueous solutions allowed the optimization of conditions for the preparation of loosely

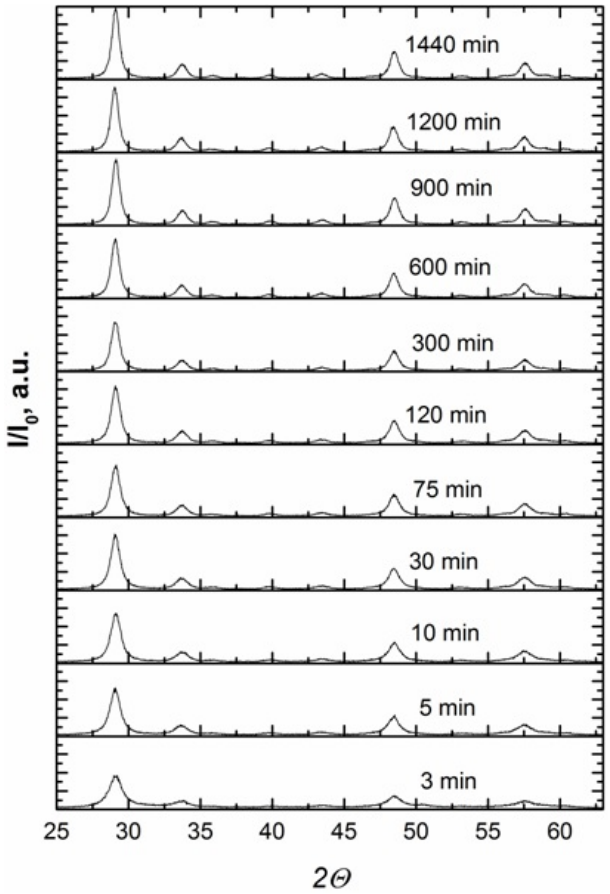

FIG. 7. X-Ray diffraction patterns of Y_2O_3 samples annealed at 600 °C for different times

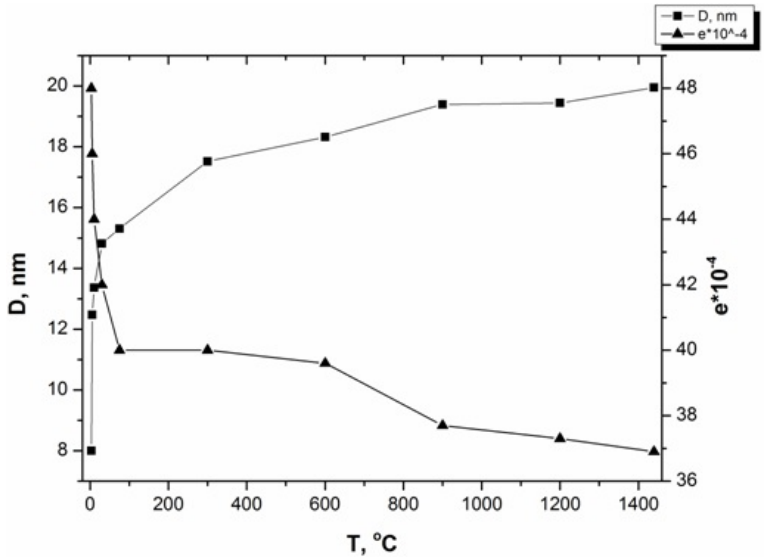

FIG. 8. Changes of microstructure parameters during isothermal annealing at 600 °C (squares — the size of the domains of coherent scattering (nm); triangles — microdeformations)

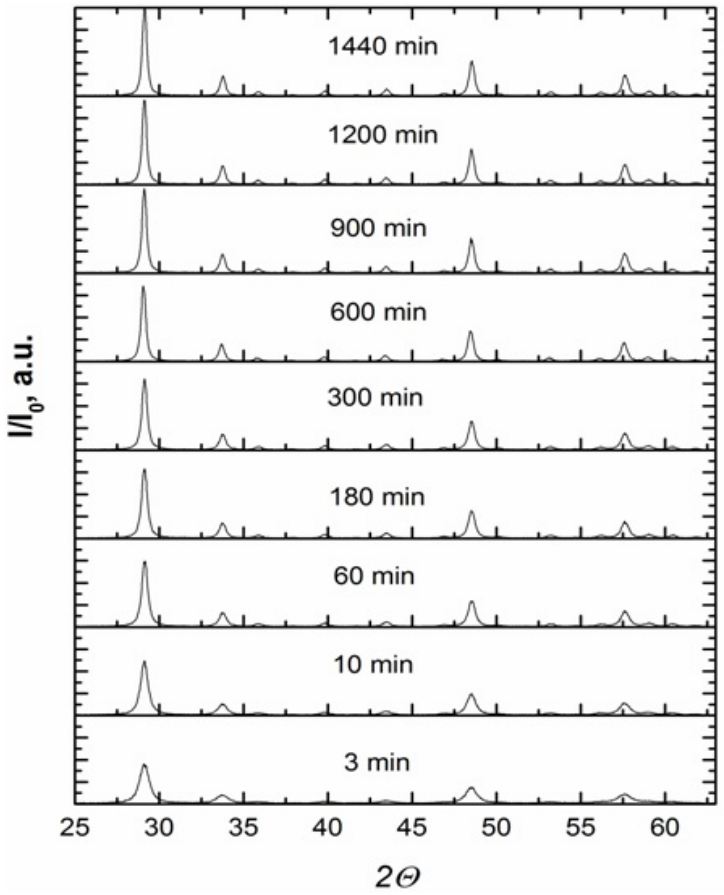

FIG. 9. X-Ray diffraction patterns of Y_2O_3 samples annealed at 800 °C for different time)

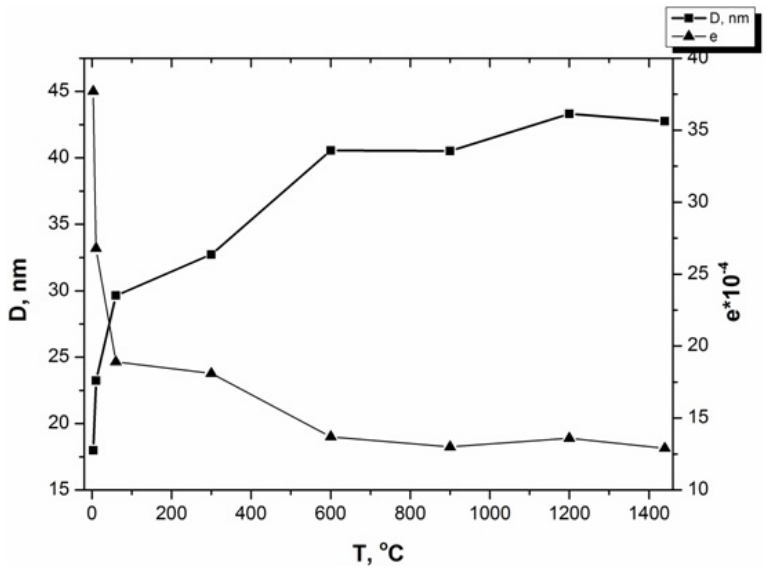

FIG. 10. Changes of the microstructure parameters in the course of isothermal annealing at 800 °C (squares — the size of the domains of coherent scattering (nm); triangles — microdeformations)

aggregated $Y_2(OH)_{6-x}(NO_3)_x \cdot nH_2O$. Thermal decomposition of this compound under controlled annealing permitted the generation of yttria nanoparticles with desirable microstructure, thus making the material widely available for the manufacture of yttria optical ceramics.

References

[1] J. Sanghera, et al. Ceramic laser materials. *Proc. SPIE*, **7912**, P. 79121Q (2011).

[2] V. Lupei, et al. Single crystal and transparent ceramic Nd-doped oxide laser materials: a comparative spectroscopic investigation. *Journal of Alloys and Compounds*, **380**, P. 61–70 (2004).

[3] C. Greskovich, J.P. Chernoch. Polycrystalline ceramic lasers. *J. Appl. Phys.*, **44**, P. 4599–4606 (1973).

[4] T. Ikegami, T. Mori, J. Li, Y. Moriyoshi. Fabrication of transparent yttria ceramics by the low-temperature synthesis of yttrium hydroxide. *J. Amer. Ceram. Soc.*, **85**, P. 1725–1729 (2002).

[5] J. Mouzon. *Synthesis of Yb:Y_2O_3 Nanoparticles and Fabrication of Transparent polycrystalline yttria ceramics*. Lulea University of Technology, Sweden, 126 pp. (2005).

[6] A.E. Baranchikov, V.K. Ivanov, A.V. Dmitriev, et al. Chemical transformations of basic yttrium nitrates during ultrasonic-hydrothermal treatment. *Russian J. Inorg. Chem.*,**51** (11), P. 1689–1695 (2006).

[7] V.K. Ivanov, A.E. Baranchikov, A.S. Vanetsev, et al. Effect of hydrothermal and ultrasonic/hydrothermal treatment on the phase composition and micromorphology of yttrium hydroxocarbonate. *Russian J. Inorg. Chem.*, **52** (9), P. 1321–1327 (2007).

[8] M.A. Uslamina. *Ultradisperse precursors for transparent Y_2O_3:Nd^{3+} ceramics*. Mendeleev Russsian Chemical Technology University, Moscow, 135 pp. (2009). (in Russian).

[9] P.P. Fedorov, V.V. Voronov, et al. Evolution of Yttria nanoparticle ensembles. *Nanotecnologies in Russia*, **5** (9–10), P. 624–634 (2010).

[10] P.P. Fedorov, E.A. Tkachenko, et al. Yttrium Oxide Nanopowders from Carbonate Precursors. *Russian J. Inorg. Chem.*, **55** (6), P. 883–889 (2010).

[11] Yu.I. Pazura, Yu.I. Baumer, et al. Synthesis of Y_2O_3 and Y_2O_3:Nd^{3+} monodisperse crystalline nanospheres by homogenous precipiotation. *Functional Materials*, **17**, P. 107–113 (2010).

[12] M. Ivanov, Y. Kopilov, V. Kravchenko, S. Zayats. Sintering and optical quality of highly transparent Yb doped yttrium lanthanum oxide ceramics. *Physica Status Solidi A*, (2013) (in press).

[13] R.A. Lefever, J. Matsko. Transparent yttrium oxide ceramics. *Mat. Res. Bull.*, **2**, P. 865–869 (1967).

[14] H.S. Roh, Y.C. Kang, H.D. Park, S.B. Park. Eu:Y_2O_3 phosphor particles prepared by spray pyrolysis from a solution containing citric acid and polyethylene glycol. *Appl. Phys. A*, **76**, P. 241–245 (2003).

[15] H.-R. Wenk, S. Matthies, L. Lutterotti. Texture analysis from diffraction spectra. *Mater. Sci. Forum*, **157–162**, P. 473–480 (1994).

[16] M. Ferrari, L. Lutterotti, et al. New opportunities in the texture and stress field by the whole pattern analysis. *Mat. Sci. Forum*, **228–231**, P. 83–88 (1996).

[17] S. Matthies, L. Lutterotti, H.-R. Wenk. Progress in combining Rietveld and QTA Algorithms on Advanced Level. Presented at ICOTOM 11, China, September 1996, P. 146–151 (1996).

[18] M. Ferrari, L. Lutterotti. Method for the simultaneous determination of anisotropic residual stresses and texture by X-ray diffraction. *J. Appl. Phys.*, **76** (11), P. 7246–55 (1994).

[19] L. Lutterotti, P. Scardi. Simultaneous Structure and Size-Strain Refinement by the Rietveld Method. *J. Appl. Cryst.*, **23**, P. 246–252 (1990).